ACS OMEGA

Open Access

http://pubs.acs.org/journal/acsodf

Article

Understanding the Growth Mechanism of Thiol-Conjugated Au_{25} Cluster

Chunhui Liu,* Haiying He, Ravindra Pandey, and Shashi P. Karna*

Cite This: *ACS Omega* 2025, 10, 14150−14156

Read Online

ACCESS | Metrics & More | Article Recommendations | Supporting Information

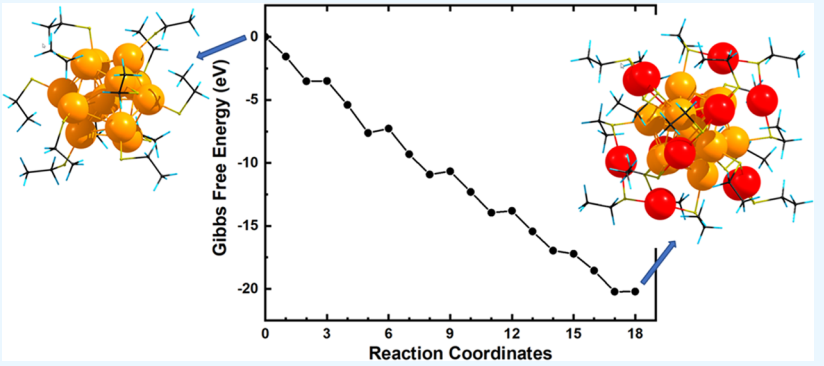

ABSTRACT: The synthesis of ligand-conjugated gold nanoclusters has attracted significant attention due to its ability to achieve precise control over cluster size selectivity. Among these, $Au_{25}(SR)_{18}^{-}$, where R represents an alkyl group, is one of the earliest being synthesized with a very high yield, although its growth mechanism is yet to be fully understood. Using density functional theory, we present the results of a theoretical investigation on the growth process of $Au_{25}(SR)_{18}^{-}$, beginning from $Au_{13}(SR)_{12}^{-}$. Our findings indicate that the sulfur atoms in the core structure of $Au_{13}(SR)_{12}^{-}$ preferentially bond with Au-thiol monomers. Monomers attached to two adjacent triangular faces form a staple motif of the gold−sulfur chain, releasing a single linear thiol radical. These reactions occur along the six mutually perpendicular ridges of the Au_{13} core. The remaining eight triangular faces, linked with linear alkyl parts, cannot bind additional Au-thiol monomers, stopping cluster growth. Furthermore, the capping gold−sulfur chains play a protective role for the core, facilitating the stable formation of the $Au_{25}(SR)_{18}^{-}$cluster, as confirmed experimentally.

1. INTRODUCTION

Metal clusters possess unique properties that differ from their bulk counterparts, mainly due to the distinct configuration of a few atoms and the confinement of charge carriers. For example, gold nanoclusters, stabilized in the colloidal form through thiolate molecules, have found applications in biomarkers, targeted drug delivery, catalysis, solar energy conversion etc.,[1−5] due to their unique electronic properties.

Studies of bulk gold surfaces coated with the thiol self-assembled monolayers[6] led to using thiols to synthesize and functionalize Au clusters with a size of 1.5−3.5 nm.[7−10] $Au_{25}(S-C_2H_4Ph)_{18}^{-}$ with a high yield (≈50%) was synthesized.[11] Building on this work, the synthesis of $Au_{38}(S-C_{12}H_{25})_{24}$[12] and $Au_{144}(SR)_{60}$ nanoclusters (where R represents $C_{12}H_{25}$ or C_2H_4Ph) was reported.[13−15] Table S1 lists a survey of ligand-protected Au clusters that have been synthesized and characterized in recent years. The overall finding emphasizes that sulfur and straight-chain alkyl ligands play an important role in facilitating the high-yield synthesis of gold clusters.

Despite many of these experimental efforts, a few studies have attempted to understand the growth mechanism of the ligand-protected Au clusters. In one of the theoretical studies, a systematic global structure search was conducted for a series of intermediate $Au_m(SR)_n$ with m and n ranging from 5 to 12, reporting preliminary nucleation behavior, gradual growth in the inner core, and the formation of staple motifs.[16] In the present study, we now go beyond the 12-atom Au cluster and address how the $Au_{25}(SR)_{18}^{-}$ cluster grows, knowing that it is one of the most important critical-sized Au clusters and has yet to be investigated. Specifically, we begin with the precursor $Au_{13}(S-C_2H_5)_{12}^{-}$, investigating its growth to $Au_{25}(S-C_2H_5)_{18}^{-}$ through energetic analysis based on density functional theory (DFT). It is to be noted that we have considered the clusters to be negatively charged as experimental[17] and theoretical[18] studies have demonstrated their enhanced stability compared to neutral clusters. Since thiolated straight-chain alkyl groups were

Received: December 19, 2024
Revised: March 4, 2025
Accepted: March 20, 2025
Published: April 1, 2025

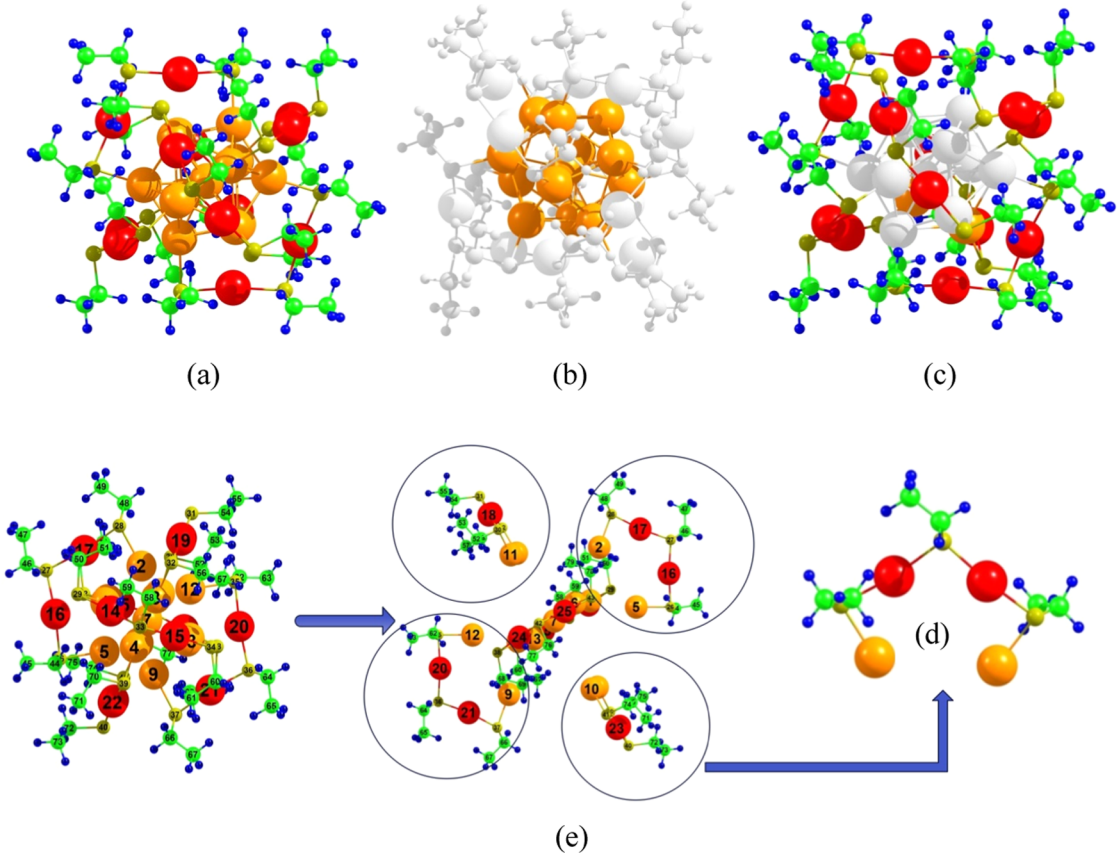

Figure 1. (a−c) The equilibrium configuration of the $Au_{25}(SR)_{18}^-$ cluster. It can be considered as a central Au atom with six gold−sulfur chains ($Au_4(SR)_3$ as shown in (d)) in six mutually perpendicular directions, as illustrated in (e) (only four are circled for a clear view). Atomic color code: Green: C; blue: H; dark yellow: S; orange: Au (core atoms); and red: Au (outer shell atoms).

commonly used as ligands in synthesis, a relatively short alkyl group, $-C_2H_5$, was selected to investigate the growth mechanism of $Au_{25}(SR)_{18}^-$.

2. COMPUTATIONAL METHOD

Electronic structure calculations were performed within DFT using the VASP program.[19−22] The PBE exchange-correlation functional[23] and the van der Waals (vdW) interactions described by the DFT-D3 method of Grimme et al.[24,25] were employed for calculations. The projector augmented wave (PAW) method and plane wave basis sets were used with energy cutoffs of 520 eV. Au is treated by the PBE+U method with U_{eff} = 4.5 eV.[26] The cluster is placed in a cubic periodic supercell of ∼30 Å to ensure negligible interaction between neighboring clusters. The total energy was converged to 10^{-6} eV, and all atoms were allowed to relax until the energy difference was below 0.001 eV. Bader charge analysis was performed to determine atomic charges within the cluster.[27]

We note that the search of the intermediate structures involves a large parameter space because of the different binding sites and configurations. This search is guided by insights into the symmetry, chemical properties, and known structure of the final product $Au_{25}(SR)_{18}^-$. Multiple isomers of the intermediate clusters were sampled, with the lowest-energy configurations selected for further analysis.

The reaction free energy ΔG of each elementary growth step was calculated based on the electronic energies and Gibbs free energy corrections. Contributions to the Gibbs free energy from the zero-point energy correction (ZPE), enthalpic temperature correction ($\int C_p\, dT$), and entropy correction ($-TS$) for the reactants, intermediates and products were adopted to calculate the reaction free energies of the elementary growth steps.

We have employed Bohn-Oppenheimer ab initio molecular dynamics[28] (AIMD) as implemented in the VASP package using the NTV ensemble. A cubic supercell of length 30 Å with an energy cutoff of 520 eV was used for the total-energy convergence. We start from the optimized structures of the reactants- the $Au_{13}(S-C_2H_5)_{12}^-$ cluster and the Au-thiol monomer ($Au-S-C_2H_5$) and place them at a sufficiently large distance to ensure no initial bonding between them. The clusters are maintained at 298 K for 1000 fs. Then, the resulting trajectory is used to analyze the structure evolution and the adsorption of the Au-thiol monomer into the nanocluster to produce a new cluster structure, $Au_{14}(S-C_2H_5)_{13}^-$ according to the proposed mechanism.

3. RESULTS AND DISCUSSION

3.1. $Au_{25}(SR)_{18}^-$ Cluster. The structural configuration of $Au_{25}(SR)_{18}^-$ is shown in Figure 1a−1c. It can be regarded as a core−shell configuration where a 13-Au core (shown in orange) and a 12-Au shell (shown in red) are conjugated with 18 ($S-C_2H_5$) ligands. The core Au atoms form a caged icosahedron, which often serves as the base for the further growth of larger clusters. More interestingly, this structure can be further dissected. Within the 13-Au icosahedron core, one central Au atom is bonded with two Au atoms (shown in orange in Figure 1d) along each of the six mutually perpendicular directions. The two Au core atoms (orange) and two other Au atoms (red) from

https://doi.org/10.1021/acsomega.4c11441
ACS Omega 2025, 10, 14150−14156

the shell are ligated by three S−C_2H_5 groups, forming a gold−sulfur chain $Au_4(S-C_2H_5)_3$, which has been identified as a staple motif to make the structure stable. In this way, the $Au_{25}(SR)_{18}^-$ structure can be considered a central Au atom with six gold−sulfur chains (i.e., anchored staple motifs) symmetrically distributed in six mutually perpendicular directions, as illustrated in Figure 1e. We will show that these characteristics of the $Au_{25}(SR)_{18}^-$ cluster are essential in the fundamental understanding of its growth mechanism.

The calculated structure of $Au_{25}(S-C_2H_5)_{18}^-$ compares well with a previous DFT study of $Au_{25}(S\text{-}CH_3)_{18}^-$.[18] The average $R(Au_{core}\text{-}Au_{core})$ and $R(Au_{core}\text{-}Au_{shell})$ are 2.94 (3.0) Å and 3.18 (3.3) Å, respectively. The average $R(Au_{core}\text{-}S)$ and $R(Au_{shell}\text{-}S)$ are 2.42 (2.45) Å and 2.33 (2.36) Å, respectively. The bond lengths of $Au_{25}(S\text{-}CH_3)_{18}^-$ reported in the previous study are in parentheses. Overall, comparing these bond lengths suggests that the Au cluster configuration weakly depends upon the length of the alkyl chain.

The $Au_{25}(S-C_2H_5)_{18}^-$ cluster has a closed electronic shell,[18] indicating high stability. Bader's charge analysis (Table S2) reveals an onion-like charge distribution with three layers- the center Au atom has a charge of −0.071 e; the out layer of the Au_{13} core carries +0.015 e per atom, while the capping shell made of six Au-ligand chains (i.e., staple motifs) carry −0.185 e per $Au_2(S-C_2H_5)_3$ chain unit. The excess negative charge is primarily on sulfur atoms. This provides a consistent picture as the superatom model.[29,30] The calculated HOMO-LOMO gap of $Au_{25}(S-C_2H_5)_{18}^-$ is 1.46 eV (Figure S1a). It aligns with the experimental absorption spectra for $Au_{25}(S-C_6H_{13})_{18}^-$ showing an apparent gap of 1.3 eV.[17] We have further calculated the projected density of states (PDOS) (Figure S1b−d) to investigate the nature of the cluster electronic states. The alkyl group (C and H) has a small contribution, while the core Au atoms make the dominant contribution to the frontier orbitals. There appears to be a large hybridization of the S and Au states for both the core and shell Au atoms, which is evidence of the strong covalent Au−S bonds in the cluster.

3.2. Growth Pathway of $Au_{25}(SR)_{18}^-$ Beginning with $Au_{13}(SR)_{12}^-$. Figure 2 displays the elementary steps considered to study the growth of $Au_{25}(SR)_{18}^-$ beginning with $Au_{13}(SR)_{12}^-$ and Au-thiol monomers (Au-SR). The initial cluster, $Au_{13}(SR)_{12}^-$, has the Au atoms form an icosahedral structure with 20 triangular faces and 12 vertex angles. The average Au−Au bond length is 2.93 Å. The outer Au atoms are capped with 12 thiol monomers (SR) by a relatively strong Au−S bond with a bond length of 2.28 Å. Since the chosen ligands ($-C_2H_5$) cannot shield the Au atoms of the cluster, allowing them to interact further with Au-thiol monomers, they can then be adsorbed onto the triangular surfaces of $Au_{13}(SR)_{12}^-$ with minimal hindrance, as shown from our AIMD simulations (Figure S2). For example, three Au atoms—labeled 1, 3, and 4—form a triangular face that links with an Au-SR monomer. Similarly, Au atoms 3 and 4, together with atom 13, form another triangular face that can link to an additional Au-SR monomer. Consequently, two Au-SR monomers attach to two adjacent triangular faces of the $Au_{13}(SR)_{12}^-$ cluster. These steps can be described by the following reactions

$$Au_{13}(S-C_2H_5)_{12}^- + (Au-S-C_2H_5) \rightarrow Au_{14}(S-C_2H_5)_{13}^- \quad (1)$$

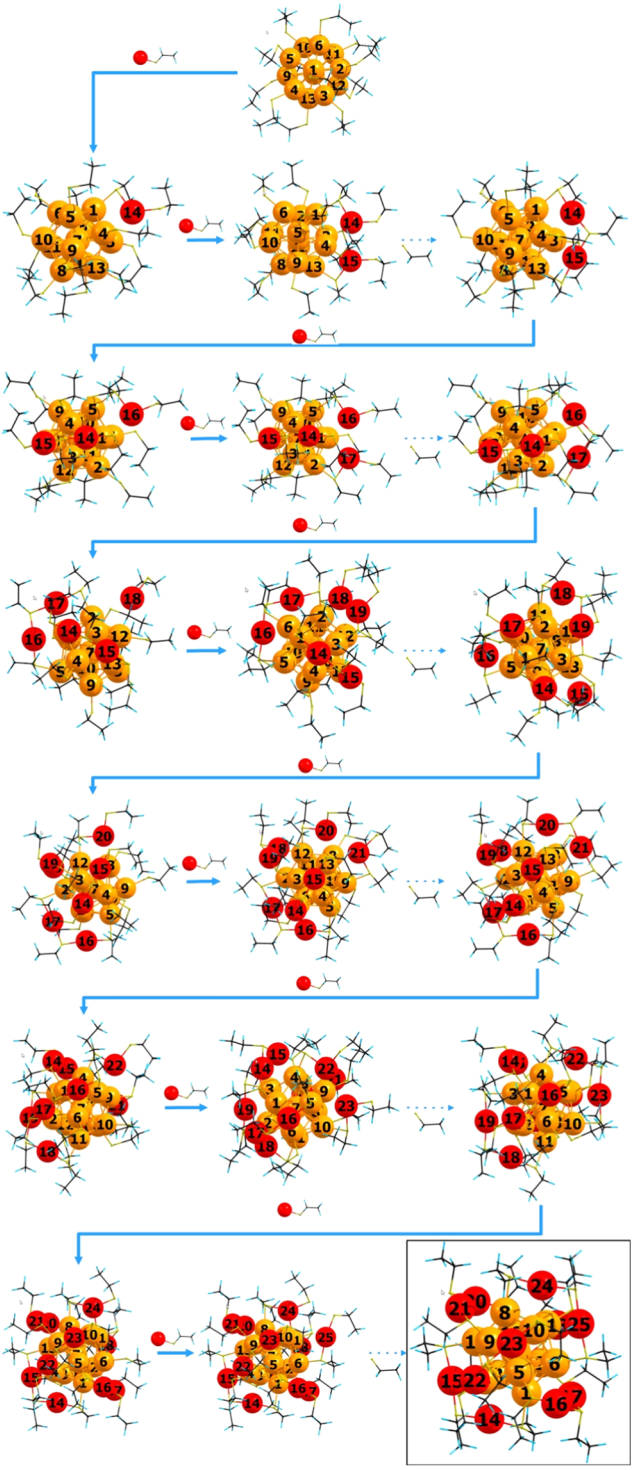

Figure 2. Intermediate cluster configurations along the pathway of the growth of $Au_{25}(SR)_{18}^-$ starting from an $Au_{13}(SR)_{12}^-$ cluster, involve adding one Au-thiol monomer (Au-SR) at a time and delinking one thiol monomer (SR) every third step. Atomic color code: black: C; blue: H; dark yellow: S; orange: Au (core); and red: Au (shell).

$$Au_{14}(S-C_2H_5)_{13}^- + (Au-S-C_2H_5) \rightarrow Au_{15}(S-C_2H_5)_{14}^- \quad (2)$$

Subsequently, the linking of two Au-SR monomers to adjacent triangular faces generates steric repulsion between

https://doi.org/10.1021/acsomega.4c11441
ACS Omega 2025, 10, 14150−14156

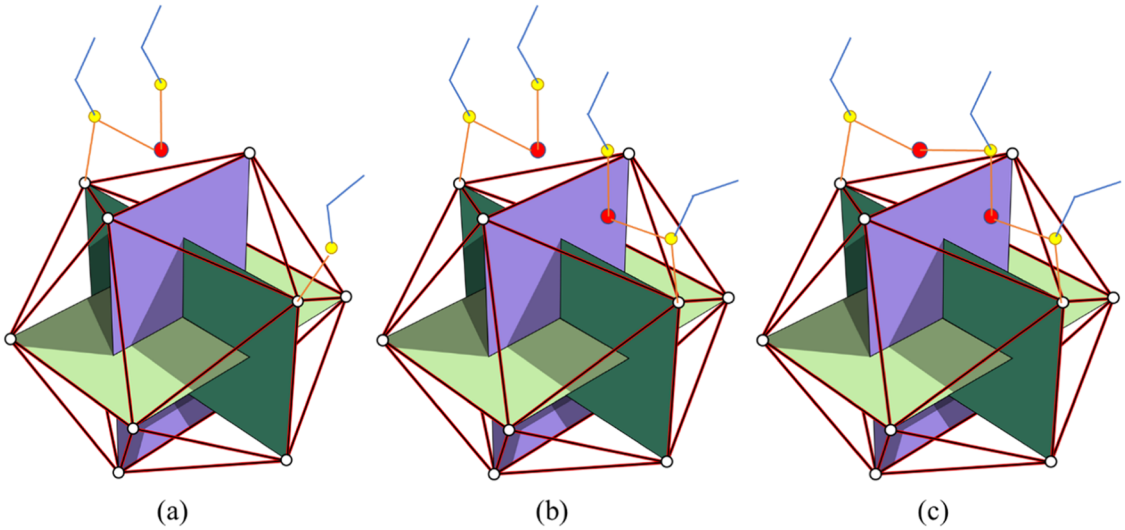

Figure 3. A schematical illustration of the formation process of the first gold−sulfur chain involving alkyl thiol ligands; (a) linking of the first Au-thiol monomer onto one triangular face of $Au_{13}(S{-}C_2H_5)_{12}^-$; (b) linking of the second Au-thiol monomer onto an adjacent triangular face; (c) interaction among the two Au-thiol monomers and delinking of one of the thiolated alkyl groups (-SR). Color code: Au_{13} core in white circles with three perpendicular planes showing its geometrical symmetry and 20 equilateral triangles; S in yellow circles; the alkyl groups in blue sticks and the linked Au atoms (shell) in red circles. Only two out of 12 of the -SR groups of $Au_{13}(S{-}C_2H_5)_{12}^-$ are shown for clarity.

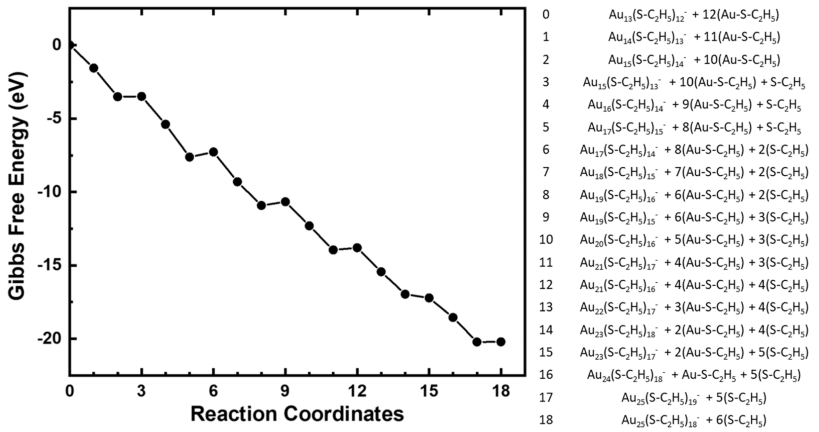

Figure 4. Computed Gibbs free energies along the growth pathway of $Au_{25}(S{-}C_2H_5)_{18}^-$. The reaction coordinate is the step number during the growth process, and zero energy is taken to be G_{LHS}, as given in eq 4.

them. This repulsion triggers the following reaction, which takes place at elevated temperatures (>350 K).

$$Au_{15}(S - C_2H_5)_{14}^- \rightarrow Au_{15}(S - C_2H_5)_{13}^- + (S - C_2H_5) \quad (3)$$

The formation of this first Au-SR-Au-SR-Au-SR-Au chain, referred to as the staple motif at the interface of $Au_{13}(SR)_{12}^-$ is schematically illustrated in Figure 3.

Figure 1e (and Figure 3c) shows that two of the four Au atoms (orange) forming the gold−sulfur chain are at the cluster's core, and the other two Au atoms (red) are linked with a thiol ligand. In the resulting cluster configuration, such a growth interface stabilizes the $Au_{15}(S{-}C_2H_5)_{13}^-$ cluster in this direction. The same linking-delinking sequence will be repeated six times along all six directions as $Au_{13}(S{-}C_2H_5)_{12}^- \rightarrow Au_{15}(S{-}C_2H_5)_{13}^- \rightarrow Au_{17}(S{-}C_2H_5)_{14}^- \rightarrow Au_{19}(S{-}C_2H_5)_{15}^- \rightarrow Au_{21}(S{-}C_2H_5)_{16}^- \rightarrow Au_{23}(S{-}C_2H_5)_{17}^- \rightarrow Au_{25}(S{-}C_2H_5)_{18}^-$. In summary, a relatively stable $Au_{25}(S{-}C_2H_5)_{18}^-$ cluster can be formed from $Au_{13}(S{-}C_2H_5)_{12}^-$ involving the steps of linking of 12 Au−S−C_2H_5) monomers and delinking of 6 S−C_2H_5. Notably, a key intermediate, $Au_{23}(S{-}c{-}C_6H_{11})_{17}$, was identified recently by a combination of experimental techniques, including ultrafast transient absorption spectroscopy.[31] Nevertheless, we also acknowledge that the reported intermediate structures represent a very plausible path and may not exclude the existence of other intermediate structures.

3.3. Energetics of the Growth of $Au_{25}(SR)_{18}^-$.

Figure 4 describes the overall growth reaction process displaying calculated free energy variation along the pathway of growing the $Au_{25}(S{-}C_2H_5)_{18}^-$ cluster from $Au_{13}(SR)_{12}^-$ (eq 4) (see Tables S3−S4 for details of the elementary steps and their reaction free energies). A negative energy difference value (i.e., G_{RHS}-G_{LHS}) represents the reaction to be exothermic.

$$Au_{13}(S - C_2H_5)_{12}^- + 12(Au - S - C_2H_5) \rightarrow Au_{25}(S - C_2H_5)_{18}^- + 6(S - C_2H_5) \quad (4)$$

$Au_{13}(SR)_{12}^-$ consists of a core of 13 Au atoms, which forms an icosahedron. Each face has three Au atoms forming an equilateral triangle, and each Au atom is connected to an

https://doi.org/10.1021/acsomega.4c11441
ACS Omega 2025, 10, 14150−14156

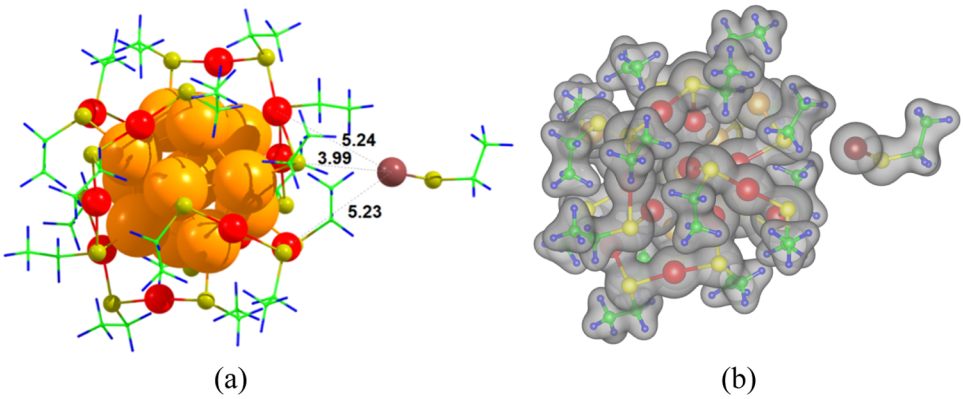

Figure 5. $Au_{25}(SR)_{18}^-$ interacting with an Au-thiol monomer: (a) structure and (b) charge density plots with the contour value being 1/20 of the computed maximum charge density; Atomic color code: Green: C; blue: H; dark yellow: S; orange: Au (core), red: Au (shell); and dark red: Au (monomer).

alkylthiol, as shown in Figure 2. The triangle face formed by three Au atoms allows a linkage of the Au-thiol monomers with the cluster. Considering that the two ends of the gold−thiol monomer are the Au atom and the alkyl tail, the Au atom can form a metallic bond with the three gold atoms at the interface and can also be combined with one of the three thiols connected to form the Au−S bond. It is worth noting that the bonding of Au-thiol monomers may vary depending on the surface coverage of the SR ligand. Furthermore, the cluster configuration distorts slightly as the Au-thiol monomer is bonded to the cluster. For instance, the distance between two Au atoms (2 and 5) of the Au_{13} core (shaded in white in Figure S3) that bind Au-thiol monomers varies as 4.81, 4.93, 5.02, 5.07, 5.04, 4.76, and 4.83 Å for 0, 2, 4, 6, 8, 10, and 12 Au-SR monomers, respectively. The degree of the structural distortion increases first and then decreases as the number of Au atoms increases. The Au-thiol monomer linked on two adjacent triangular faces (which must share one edge) interact with each other. As a result, the reaction energy varies, and the difference can reach up to 0.9 eV. The average reaction free energy during linking Au-thiol monomers is −1.73 eV with a standard deviation of ± 0.25 eV (Table S3).

The configuration space becomes crowded when two Au-thiol monomers are bonded on two adjacent triangular surfaces, sharing an edge. Subsequently, these monomers will undergo a chemical reaction; S atoms of the thiol group will approach another Au-thiol monomer to form an Au−S−Au bridge (shown in Figure 1e), and driven by this interaction, the Au-thiol monomer will break the original gold−sulfur bond. The variation of bonding during this process is illustrated in Figure 3. When the S atom in the Au-thiol monomer is bonded to a single Au atom, its binding energy is higher than when it is bonded to two Au atoms, as predicted in the chain configuration. The SR ligand also contains an unsaturated bond, making the process slightly endothermic for most of those steps (Table S3).

This facilitates the expansion of the Au cluster core. At each step, the cluster incorporates two Au-thiol monomers on two adjacent triangular faces and subsequently loses one thiol ligand, resulting in relatively stable intermediate structures. The growth continues until the sixth gold−sulfur chain is formed, resulting in a stable $Au_{25}(SR)_{18}^-$ cluster (Figure 2) after the six-step reaction process, as given in eq 5.

Each reaction step can be written as

$$Au_{13+2n}(S - C_2H_5)_{12+n}^- + 2Au - (S - C_2H_5) \rightarrow Au_{15+2n}(S - C_2H_5)_{13+n}^- + (S - C_2H_5) \quad (5)$$

where n = 0, 1, 2, 3, 4, 5 respectively.

Overall, the growth process is driven by two energetic factors: the energy required to break the Au−S bond in the Au-thiol monomer and the energy gained from forming the Au−S chain, which induces configurational distortion. The calculated free reaction energies for reactions of eq 5 are more or less constant, with an average value of −3.37 ± 0.28 eV.

After bonding with 12 Au-thiol monomers in six symmetrical directions, there are eight triangular surfaces of the $Au_{25}(SR)_{18}^-$ cluster remaining available for further linkage with additional monomers. Calculations find that adding the 19th monomer is energetically much less preferred with only a small fraction of the binding energy (−0.3 eV) as in previous steps (Table S3). Figure 5a shows that the alkyl groups of the alkylthiol monomers covering the open triangular surfaces of $Au_{25}(SR)_{18}^-$ prevent the linking of the monomer Au atom with the core Au_{13}. This is evidenced by the fact that there is a lack of charge overlap of the $Au_{25}(SR)_{18}^-$ cluster and the 19th monomer (Figure 5b). Furthermore, the S atoms of $Au_{25}(SR)_{18}^-$ are fully coordinated. Therefore, the $Au_{25}(SR)_{18}^-$ cluster is stable and stops further growing. Experimental observations support these findings, showing that such clusters can be synthesized with high yields.

Lastly, our choice of starting from a center-filled icosahedral metal core Au_{13} instead of a hollow icosahedral Au_{12} is driven by the experimental synthesis of predominantly Au_{25} nanoclusters. It is interesting to note that as the size of the metal cluster increases to 44 atoms, a hollow Ag_{12} or Au_{12} was observed in Ag_{44} and $Au_{12}Ag_{32}$ clusters.[32−34] The hollow Au_{12} core was also identified in the Au_{144} nanoclusters and associated crystals.[13,35] More recently, the hollow Cu_{12} core was observed in a polyhydrido Cu_{30} nanocluster.[36] The removal of the central metal atom in these cases is likely due to the increasing intrinsic strain owing to the Mackay icosahedral packing.[35]

Based on our calculated energetics, the $Au_{13}(SR)_{12}^-$ cluster lowers the system energy by 3.6 eV when an extra Au atom is placed at the center of the $Au_{12}(SR)_{12}^-$ cluster. This binding energy is significantly more than the average binding energy of Au atoms in the Au_{13} cluster (2.0 eV), indicating that the central Au atom greatly enhances the stability of this relatively small cluster. The Au−Au bond length is also shortened from 2.93 to 2.81 Å.

https://doi.org/10.1021/acsomega.4c11441
ACS Omega 2025, 10, 14150−14156

To explore the alternative path of growing $Au_{24}(SR)_{18}^-$ from $Au_{12}(SR)_{12}^-$, we have carried out similar calculations starting from $Au_{12}(SR)_{12}^-$ (see Figure S4). It was found that the adsorption of the first two Au-thiol monomers is stable, and so is the delinking of one of the thiolated alkyl groups to form $Au_{14}(S{-}C_2H_5)_{13}^-$. The reaction energies of the first three steps (−1.7, −2.2 eV and ≈0.05 eV) are very similar to that of $Au_{13}(SR)_{12}^-$ to $Au_{15}(SR)_{13}^-$ (−1.6, −2.0 eV and ≈0.02 eV). However, the core structure becomes largely disturbed with the adsorption of the third Au-thiol monomer and cannot maintain the hollow icosahedral core structure anymore. It is likely due to the added asymmetric strain that the hollow core cannot sustain any more. The center-filled Au_{13} kernel can stabilize the nanocluster structure more during the growth from $Au_{13}(SR)_{12}^-$ to $Au_{25}(SR)_{18}^-$, *i.e.*, adding the first layer of Au−S staple motifs.

4. CONCLUSIONS

Our theoretical study based on the density functional theory has provided further insights into the growth mechanism of the thiol-conjugated gold nanocluster $Au_{25}(SR)_{18}^-$, the most achievable product in synthesizing gold clusters. The results suggest that the growth process starting with an $Au_{13}(SR)_{12}^-$ cluster and Au-thiol alkyl monomers (i.e., Au-SC_2H_5) is energetically favorable, with 17 distinct intermediate structures predicted. Linking two Au-thiol monomers at the adjacent triangular faces of $Au_{13}(SR)_{12}^-$ leads to interactions that release a linear alkylthiol, forming a chain-type staple motif anchored on two core Au atoms (i.e., Au-SR-Au-SR-Au-SR-Au). This process sequentially yields six thermodynamically stable Au-thiol chain structures around the Au_{13} core. The remaining eight triangular faces, linked with linear alkyl parts, cannot bind additional Au-thiol monomers, stopping cluster growth.

Therefore, it is notable that the geometry of the precursor (i.e., icosahedral Au_{13}) is critical in determining the shape and size of the growing cluster. It adds a new dimension to our understanding of the growth and stability of ligand-conjugated gold nanoclusters, which goes beyond the consideration of electronic configurations.[29,30]

■ ASSOCIATED CONTENT

Supporting Information

The Supporting Information is available free of charge at https://pubs.acs.org/doi/10.1021/acsomega.4c11441.

Literature survey of thiolate ligand (SR)-conjugated Au nanoclusters previously synthesized; electronic properties of $Au_{25}(S{-}C_2H_5)_{18}^-$; AIMD simulations for the first adsorption step $Au_{13}(S{-}C_2H_5)_{12}^-$ + $(Au{-}S{-}C_2H_5)$ → $Au_{14}(S{-}C_2H_5)_{13}^-$; computed reaction free energies along the growth path from $Au_{13}(S{-}C_2H_5)_{12}^-$ to $Au_{25}(S{-}C_2H_5)_{18}^-$; distortion of the Au_{13} core with formation of the Au−S chains; calculated initial reaction steps of growing the Au cluster with a hollow icosahedral Au_{12} core (PDF)

■ AUTHOR INFORMATION

Corresponding Authors

Chunhui Liu − *Department of Physics, Michigan Technological University, Houghton, Michigan 49931, United States;* orcid.org/0009-0002-9770-3177; Email: chuliu@mtu.edu

Shashi P. Karna − *US Army Research Laboratory, Weapons and Materials Research Directorate, ATTN: RDRL-WM, Aberdeen Proving Ground, Maryland 21005-5069, United States;* orcid.org/0000-0002-0844-2714; Email: shashi.p.karna.civ@army.mil

Authors

Haiying He − *Department of Physics and Astronomy, Valparaiso University, Valparaiso, Indiana 46383, United States;* orcid.org/0000-0002-3493-2784

Ravindra Pandey − *Department of Physics, Michigan Technological University, Houghton, Michigan 49931, United States;* orcid.org/0000-0002-2126-1985

Complete contact information is available at: https://pubs.acs.org/10.1021/acsomega.4c11441

Notes

The authors declare no competing financial interest.

■ ACKNOWLEDGMENTS

We thank Dr. S. Gowtham for helpful discussions. The Funding from the Army Research Office through grant no. W911NF-14-2-0088 for partial support of this research is gratefully acknowledged. The Portage and Superior high-performance computing clusters at Michigan Technological University were utilized in obtaining the results presented in this work.

■ REFERENCES

(1) Jin, R.; Zeng, C.; Zhou, M.; Chen, Y. Atomically Precise Colloidal Metal Nanoclusters and Nanoparticles: Fundamentals and Opportunities. *Chem. Rev.* **2016**, *116* (18), 10346−10413.

(2) Nasrollahpour, H.; Sánchez, B. J.; Sillanpää, M.; Moradi, R. Metal Nanoclusters in Point-of-Care Sensing and Biosensing Applications. *ACS Appl. Nano Mater.* **2023**, *6* (14), 12609−12672.

(3) Mordini, D.; Mavridi-Printezi, A.; Menichetti, A.; Cantelli, A.; Li, X.; Montalti, M. Luminescent Gold Nanoclusters for Bioimaging: Increasing the Ligand Complexity. *Nanomaterials* **2023**, *13* (4), 648.

(4) Lu, L.; Zou, S.; Fang, B. The Critical Impacts of Ligands on Heterogeneous Nanocatalysis: A Review. *ACS Catal.* **2021**, *11* (10), 6020−6058.

(5) Devadas, M. S.; Kim, J.; Sinn, E.; Lee, D.; Goodson, T., III; Ramakrishna, G. Unique Ultrafast Visible Luminescence in Monolayer-Protected Au_{25} Clusters. *J. Phys. Chem. C* **2010**, *114* (51), 22417−22423.

(6) Bain, C. D.; Troughton, E. B.; Tao, Y. T.; Evall, J.; Whitesides, G. M.; Nuzzo, R. G. Formation of monolayer films by the spontaneous assembly of organic thiols from solution onto gold. *J. Am. Chem. Soc.* **1989**, *111* (1), 321−335.

(7) Mirkin, C. A.; Letsinger, R. L.; Mucic, R. C.; Storhoff, J. J. A DNA-based method for rationally assembling nanoparticles into macroscopic materials. *Nature* **1996**, *382* (6592), 607−609.

(8) Brust, M.; Walker, M.; Bethell, D.; Schiffrin, D. J.; Whyman, R. Synthesis of thiol-derivatised gold nanoparticles in a two-phase Liquid−Liquid system. *J. Chem. Soc., Chem. Commun.* **1994**, *0* (7), 801−802.

(9) Alvarez, M. M.; Khoury, J. T.; Schaaff, T. G.; Shafigullin, M.; Vezmar, I.; Whetten, R. L. Critical sizes in the growth of Au clusters. *Chem. Phys. Lett.* **1997**, *266* (1), 91−98.

(10) Whetten, R. L.; Khoury, J. T.; Alvarez, M. M.; Murthy, S.; Vezmar, I.; Wang, Z. L.; Stephens, P. W.; Cleveland, C. L.; Luedtke, W. D.; Landman, U. Nanocrystal gold molecules. *Adv. Mater.* **1996**, *8* (5), 428−433.

(11) Zhu, M.; Lanni, E.; Garg, N.; Bier, M. E.; Jin, R. Kinetically Controlled, High-Yield Synthesis of Au_{25} Clusters. *J. Am. Chem. Soc.* **2008**, *130* (4), 1138−1139.

(12) Qian, H.; Zhu, M.; Andersen, U. N.; Jin, R. Facile, Large-Scale Synthesis of Dodecanethiol-Stabilized Au_{38} Clusters. *J. Phys. Chem. A* **2009**, *113* (16), 4281−4284.

(13) Yan, N.; Xia, N.; Liao, L.; Zhu, M.; Jin, F.; Jin, R.; Wu, Z. Unraveling the long-pursued Au_{144} structure by x-ray crystallography. *Sci. Adv.* **2018**, *4* (10), No. eaat7259.
(14) Qian, H.; Jin, R. Controlling Nanoparticles with Atomic Precision: The Case of $Au_{144}(SCH_2CH_2Ph)_{60}$. *Nano Lett.* **2009**, *9* (12), 4083−4087.
(15) Qian, H.; Jin, R. Ambient Synthesis of $Au_{144}(SR)_{60}$ Nanoclusters in Methanol. *Chem. Mater.* **2011**, *23* (8), 2209−2217.
(16) Liu, C.; Pei, Y.; Sun, H.; Ma, J. The Nucleation and Growth Mechanism of Thiolate-Protected Au Nanoclusters. *J. Am. Chem. Soc.* **2015**, *137* (50), 15809−15816.
(17) Negishi, Y.; Chaki, N. K.; Shichibu, Y.; Whetten, R. L.; Tsukuda, T. Origin of Magic Stability of Thiolated Gold Clusters: A Case Study on $Au_{25}(SC_6H_{13})_{18}$. *J. Am. Chem. Soc.* **2007**, *129* (37), 11322−11323.
(18) Akola, J.; Walter, M.; Whetten, R. L.; Häkkinen, H.; Grönbeck, H. On the Structure of Thiolate-Protected Au_{25}. *J. Am. Chem. Soc.* **2008**, *130* (12), 3756−3757.
(19) Kresse, G.; Furthmüller, J. Efficiency of ab-initio total energy calculations for metals and semiconductors using a plane-wave basis set. *Comput. Mater. Sci.* **1996**, *6* (1), 15−50.
(20) Kresse, G.; Hafner, J. Ab initio molecular-dynamics simulation of the liquid-metal–amorphous-semiconductor transition in germanium. *Phys. Rev. B* **1994**, *49* (20), 14251−14269.
(21) Kresse, G.; Hafner, J. Ab initio molecular dynamics for liquid metals. *Phys. Rev. B* **1993**, *47* (1), 558−561.
(22) Kresse, G.; Furthmuller, J. Efficient iterative schemes for ab initio total-energy calculations using a plane-wave basis set. *Phys. Rev. B* **1996**, *54* (16), 11169−11186.
(23) Perdew, J. P.; Burke, K.; Ernzerhof, M. Generalized gradient approximation made simple. *Phys. Rev. Lett.* **1996**, *77* (18), 3865−3868.
(24) Grimme, S.; Antony, J.; Ehrlich, S.; Krieg, H. A consistent and accurate ab initio parametrization of density functional dispersion correction (DFT-D) for the 94 elements H-Pu. *J. Chem. Phys.* **2010**, *132* (15), No. 154104.
(25) Grimme, S.; Ehrlich, S.; Goerigk, L. Effect of the damping function in dispersion corrected density functional theory. *J. Comput. Chem.* **2011**, *32* (7), 1456−1465.
(26) Dudarev, S. L.; Botton, G. A.; Savrasov, S. Y.; Humphreys, C. J.; Sutton, A. P. Electron-energy-loss spectra and the structural stability of nickel oxide: An LSDA+U study. *Phys. Rev. B* **1998**, *57* (3), 1505−1509.
(27) Sanville, E.; Kenny, S. D.; Smith, R.; Henkelman, G. Improved grid-based algorithm for Bader charge allocation. *J. Comput. Chem.* **2007**, *28* (5), 899−908.
(28) Payne, M. C.; Teter, M. P.; Allan, D. C.; Arias, T. A.; Joannopoulos, J. D. Iterative minimization techniques for ab initio total-energy calculations: molecular dynamics and conjugate gradients. *Rev. Mod. Phys.* **1992**, *64* (4), 1045−1097.
(29) Bergeron, D. E.; Roach, P. J.; Castleman, A. W., Jr.; Jones, N. O.; Khanna, S. N. Al cluster superatoms as halogens in polyhalides and as alkaline earths in iodide salts. *Science* **2005**, *307* (5707), 231−235.
(30) Walter, M.; Akola, J.; Lopez-Acevedo, O.; Jadzinsky, P. D.; Calero, G.; Ackerson, C. J.; Whetten, R. L.; Grönbeck, H.; Häkkinen, H. A unified view of ligand-protected gold clusters as superatom complexes. *Proc. Natl. Acad. Sci. U.S.A.* **2008**, *105* (27), 9157−9162.
(31) Gratious, S.; Afreen; Mahal, E.; Thomas, J.; Saha, S.; Nair, A. S.; Adarsh, K. V.; Pathak, B.; Mandal, S. "Visualizing" the partially reversible conversion of gold nanoclusters via the $Au_{23}(S\text{-}c\text{-}C_6H_{11})_{17}$ intermediate. *Chem. Sci.* **2024**, *15* (25), 9823−9829.
(32) Desireddy, A.; Conn, B. E.; Guo, J.; Yoon, B.; Barnett, R. N.; Monahan, B. M.; Kirschbaum, K.; Griffith, W. P.; Whetten, R. L.; Landman, U.; Bigioni, T. P. Ultrastable silver nanoparticles. *Nature* **2013**, *501* (7467), 399−402.
(33) Yang, H.; Wang, Y.; Huang, H.; Gell, L.; Lehtovaara, L.; Malola, S.; Häkkinen, H.; Zheng, N. All-thiol-stabilized Ag44 and $Au_{12}Ag_{32}$ nanoparticles with single-crystal structures. *Nat. Commun.* **2013**, *4* (1), No. 2422.
(34) Yang, H.; Wang, Y.; Yan, J.; Chen, X.; Zhang, X.; Häkkinen, H.; Zheng, N. Structural Evolution of Atomically Precise Thiolated Bimetallic $[Au_{12+n}Cu_{32}(SR)_{30+n}]^{4-}$ (n = 0, 2, 4, 6) Nanoclusters. *J. Am. Chem. Soc.* **2014**, *136* (20), 7197−7200.
(35) Lopez-Acevedo, O.; Akola, J.; Whetten, R. L.; Grönbeck, H.; Häkkinen, H. Structure and Bonding in the Ubiquitous Icosahedral Metallic Gold Cluster $Au_{144}(SR)_{60}$. *J. Phys. Chem. C* **2009**, *113* (13), 5035−5038.
(36) Barik, S. K.; Huo, S.-C.; Wu, C.-Y.; Chiu, T.-H.; Liao, J.-H.; Wang, X.; Kahlal, S.; Saillard, J.-Y.; Liu, C. W. Polyhydrido Copper Nanoclusters with a Hollow Icosahedral Core: $[Cu_{30}H_{18}\{E_2P\text{-}(OR)_2\}_{12}]$ (E = S or Se; R = *n*Pr, *i*Pr or *i*Bu). *Chem. - Eur. J.* **2020**, *26* (46), 10471−10479.

https://doi.org/10.1021/acsomega.4c11441
ACS Omega 2025, 10, 14150−14156